Signatures of tunable Majorana-fermion edge states

Rakesh P. Tiwari[1], U. Zülicke[2] and C. Bruder[1]

[1] Department of Physics, University of Basel, Klingelbergstrasse 82, CH-4056 Basel, Switzerland
[2] School of Chemical and Physical Sciences and MacDiarmid Institute for Advanced Materials and Nanotechnology, Victoria University of Wellington, PO Box 600, Wellington 6140, New Zealand

E-mail: `rakesh.tiwari@unibas.ch`

Abstract. Chiral Majorana-fermion modes are shown to emerge as edge excitations in a superconductor–topological-insulator hybrid structure that is subject to a magnetic field. The velocity of this mode is tunable by changing the magnetic-field magnitude and/or the superconductor's chemical potential. We discuss how quantum-transport measurements can yield experimental signatures of these modes. A normal lead coupled to the Majorana-fermion edge state through electron tunneling induces resonant Andreev reflections from the lead to the grounded superconductor, resulting in a distinctive pattern of differential-conductance peaks.

1. Introduction

The possibility to create and study Majorana quasiparticles in condensed-matter systems has become a focus of intense attention in recent years [1, 2, 3, 4, 5, 6]. Spatially localized versions of such excitations have been predicted to exist, e.g., in the $\nu = 5/2$ quantum-Hall state [7, 8], p-wave superconductors [9] such as strontium ruthenate [10, 11, 12], and semiconductor-superconductor heterostructures [13, 14, 15]. Zero-bias conductance anomalies [16, 17, 18, 19] associated with Majorana quasiparticles have been measured recently [20, 21, 22, 23] (see, however, Ref. [24]), and observations of an unconventional Josephson effect [25] mediated by these excitations have also been reported [26, 27].

Chiral Majorana modes can also be realized as edge states in hybrid structures formed from a topological insulator [28, 29] (TI), an s-wave superconductor (S), and a ferromagnetic insulator [30, 31, 32]. The requirement of broken time-reversal symmetry and gapped excitation spectrum for the surface states in the TI is fulfilled by proximity to a ferromagnetic insulator [31, 32] or Zeeman splitting due to a magnetic field [30]. In an alternative realization, Landau quantization of the surface states' orbital motion in a uniform perpendicular magnetic field could be the origin of the gap and breaking of time-reversal symmetry [33]. This setup avoids materials-science challenges associated with the fabrication of the hybrid structures involving three different kinds of materials and has new features enabling the manipulation of the Majorana excitation's properties. It was shown in Ref. [33] that the velocity of the chiral Majorana mode (CMM) can be tuned by changing the magnitude of the external magnetic field. In this article, we further explore the properties of this tunable Majorana excitation and its signatures in typical transport experiments. We show that a normal lead coupled to this tunable CMM through electron tunneling would measure a differential conductance that oscillates as the magnitude of the external magnetic field is changed. The oscillations in the conductance arise due to the velocity tunability of this CMM. Recently, it has been proposed that this velocity tunability could be used for adiabatic quantum pumping induced by Majorana fermions revealing the chiral nature of these modes [34]. Some crucial aspects of interferometry with these chiral Majorana modes are highlighted in Ref. [35].

The remainder of this paper is organized as follows. In Sec. 2, we describe the specific interferometer-like sample geometry where Landau-quantization-induced CMMs could be probed by quantum-transport experiments. In Sec. 3, we discuss the electronic properties of a S–TI interface that is subject to a magnetic field, showing the existence of Andreev edge states [36, 37] and emergence of a Majorana excitation amongst them [33]. In Sec. 4, we apply the results of Sec. 3 to elucidate the properties of the CMM that is present in the particular sample geometry considered here. We then present numerical results for the conductance of the system in Sec. 5, revealing the signatures of the CMM. The final Section 6 gives a brief discussion of experimental parameters and the conclusions.
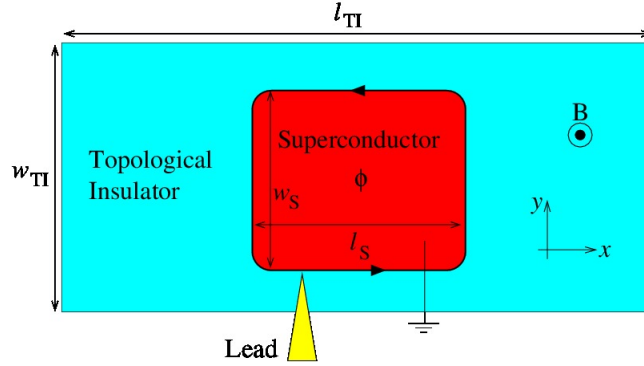
Figure 1. Schematics of the sample layout. The red region on the surface of a topological insulator denotes the S region that is induced via proximity effect due to a planar contact with an *s*-wave superconductor. The chiral Majorana mode (CMM) emerges at the boundary of this S region. The yellow triangle denotes an ideal normal electronic lead that is coming from the *z*–direction and couples to the CMM via electron tunneling. The superconductor is grounded, and a perpendicular external magnetic field of magnitude B is applied along the *z*–axis.

2. Setup of the superconductor–topological-insulator hybrid structure

Figure 1 illustrates the proposed sample geometry. The massless-Dirac-like surface states of a bulk three-dimensional TI material occupy the xy plane. A planar contact with a superconductor (indicated by the red region in the center of the TI surface) induces a pair potential for this part of the TI surface (henceforth called the S region), while a uniform perpendicular magnetic field $\mathbf{B} = B\hat{\mathbf{z}}$ is present in the rest of the surface (the N region of the TI surface). We assume the magnetic field to create a finite number of vortices in the S part and neglect Zeeman splitting throughout. (A more detailed theoretical treatment of effects due to the finite magnetic field in S can be developed along the lines of previous studies [38, 39].) The dimensions of the S and N regions are denoted by $l_S \times w_S$ and $l_{TI} \times w_{TI}$ respectively. We assume

$$\{l_{TI}, w_{TI}, l_S, w_S, l_{TI} - l_S, w_{TI} - w_S\} \gg l_B \,, \tag{1}$$

where $l_B = \sqrt{\hbar/|eB|}$ denotes the magnetic length. The cyclotron motion of charge carriers in the N region hybridizes with Andreev reflection from the interface with the S region. As shown in Ref. [33], this results in the formation of chiral Dirac-Andreev edge states, similar to the ones discussed previously for an S–graphene hybrid structure [36]. The quantum description of these edge channels reveals that one of them is associated with a chiral Majorana fermion mode with tunable velocity and guiding-center-dependent electric charge.

We now consider the situation where this CMM is tunnel-coupled to an ideal normal electronic lead coming from the z–direction, e.g., as shown in Fig. 1. The interior of the S region may accommodate n_v number of vortices, each permitting a magnetic flux quantum threading through and containing a Majorana bound state. The chiral Majorana fermion traveling around the boundary of the S region picks up a phase that

contains information about the number of vortices and the velocity of the mode before scattering into the normal lead. Before calculating the differential conductance in our setup, we compute its excitation spectrum and demonstrate the presence of the CMM along the boundary of the S region.

3. Theoretical description of the S–TI interface in a magnetic field

Single-particle excitations in the S–N heterostructure made from TI surface states can be described by the Dirac-Bogoliubov-de Gennes (DBdG) equation [36, 30, 33]

$$
\begin{pmatrix} H_D(\mathbf{r}) - \mu & \Delta(\mathbf{r})\,\sigma_0 \\ \Delta^*(\mathbf{r})\,\sigma_0 & \mu - \mathcal{T}H_D(\mathbf{r})\,\mathcal{T}^{-1} \end{pmatrix} \Psi(\mathbf{r}) = \varepsilon\Psi(\mathbf{r})\,,
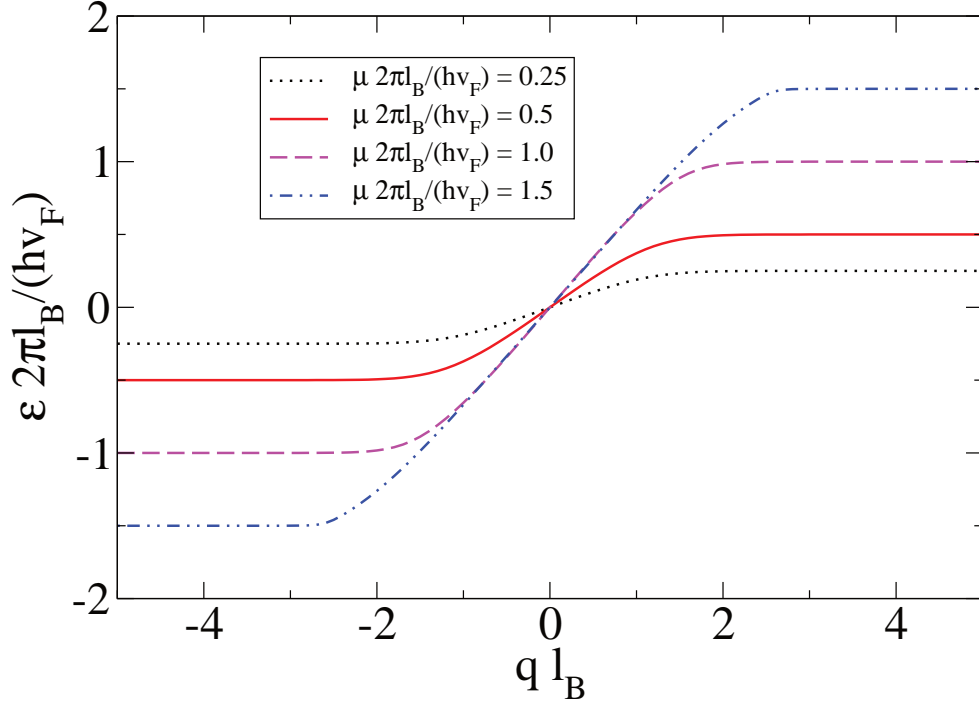\tag{2}
$$

where the pair potential $\Delta(\mathbf{r}) = \mathrm{e}^{i\theta}\Delta_0$ is finite only in the S region, $\sigma_0 \equiv \mathbb{I}_{2\times2}$ denoted the two-dimensional identity matrix, and $H_D(\mathbf{r}) = v_F[\mathbf{p} + e\mathbf{A}(\mathbf{r})] \cdot \boldsymbol{\sigma}$ is the massless-Dirac Hamiltonian for the TI surface states. The position $\mathbf{r} \equiv (x, y)$ and momentum $\mathbf{p} \equiv -i\hbar(\partial_x, \partial_y)$ are restricted to the TI surface. $\boldsymbol{\sigma}$ is the vector of Pauli matrices acting in spin space. Furthermore, $\mathcal{T}$ denotes the time-reversal operator, $-e$ the electron charge, and $\mathbf{A}$ the vector potential associated with the magnetic field $\mathbf{B} = \nabla \times \mathbf{A}$. The excitation energy ε is measured relative to the chemical potential μ of the superconductor, with the absolute zero of the energy set to be at the Dirac (i.e., neutrality) point of the TI surface states. The wave function Ψ in Eq. (2) is a spinor in Dirac-Nambu space, which can be expressed explicitly in terms of spin-resolved amplitudes as $\Psi = (u_\uparrow, u_\downarrow, v_\downarrow, -v_\uparrow)^T$. As we will confirm later, the zero-energy solution of the DBdG equation localized at the boundary between the S and the N regions constitutes the chiral Majorana excitation in our system.

To describe the uniform perpendicular magnetic field in the N region, we adopt the Landau gauge $\mathbf{A} = B\,x\,\hat{\mathbf{y}}$. To explicitly verify the presence of these Majorana excitations at the boundary of our S-N heterostructure, we restrict ourselves to the right boundary of the system. Assuming that the various lengths in our system satisfy Eq. (1), we model this right boundary as a one-dimensional edge ($x = 0$) between two half planes. The left half-plane ($x < 0$) represents the S region and the right half plane ($x > 0$) represents the N region. Then the momentum $\hbar q$ parallel to the interface (i.e., in $\hat{\mathbf{y}}$ direction) is a good quantum number of the DBdG Hamiltonian, and a general eigenspinor is of the form

$$
\Psi_{nq}(\mathbf{r}) = \mathrm{e}^{\frac{i\theta}{2}\,\sigma_0\otimes\tau_z}\,\mathrm{e}^{iqy}\,\Phi_{nq}(x)\,.
\tag{3}
$$

Here τ_z is a Pauli matrix acting in Nambu space, σ_0 the identity in spin space, and n enumerates the energy (Landau) levels for a fixed q. The spinors $\Phi_{nq}(x)$ are solutions of the one-dimensional (1D) DBdG equation $\mathcal{H}(q)\,\Phi_{nq}(x) = \varepsilon\,\Phi_{nq}(x)$, with

$$
\mathcal{H}(q) = \hbar v_{\mathrm{F}}\left\{\sigma_x \otimes \tau_z(-i)\partial_x + \sigma_y \otimes \left[\tau_z\,q + \tau_0\,\frac{eB}{\hbar}\,x\,\Theta(x)\right]\right\}
$$
$$
- \mu\,\sigma_0 \otimes \tau_z + \Delta_0\,\Theta(-x)\,\sigma_0 \otimes \tau_x\,,
\tag{4}
$$

Figure 2. Dispersion relation ε_{nq} of single-particle excitations at the S–N junction on a TI surface that is subject to a strong perpendicular magnetic field. Only the zeroth Landau level is shown for various values of μ as indicated in the legend. The magnitude of the pair potential is $\Delta_0 = 5\hbar v_F/l_B$, and $l_B \equiv \sqrt{\hbar/|eB|}$ denotes the magnetic length.

where the τ_j are Pauli matrices acting in Nambu space, and τ_0 is the identity matrix in Nambu space. The spectrum of Landau-level (LL) eigenenergies ε_{nq} and the explicit expressions for $\Phi_{nq}(x)$ in the N and S regions can then be obtained by demanding the continuity of the wavefunction at the S–N interface.

The functional form of the solutions to this 1D DBdG equation decaying for $x \to \infty$ (in the region $x > 0$) can be expressed as

$$\Psi(x, y) = e^{iqy} \begin{pmatrix} -iC_e e^{-(x+q)^2/2}(\mu + \varepsilon)H_{(\mu+\varepsilon)^2/2-1}(x+q)e^{i\phi/2} \\ C_e e^{-(x+q)^2/2}H_{(\mu+\varepsilon)^2/2}(x+q)e^{i\phi/2} \\ C_h e^{-(x-q)^2/2}H_{(\mu-\varepsilon)^2/2}(x-q)e^{-i\phi/2} \\ -iC_h e^{-(x-q)^2/2}(\mu - \varepsilon)H_{(\mu-\varepsilon)^2/2-1}(x-q)e^{-i\phi/2} \end{pmatrix}, \quad (5)$$

with $H_\alpha(x)$ denoting the Hermite function [36]. The complete solution is then obtained from the requirement of particle-current conservation across the interface. Similar to Ref. [36] we find

$$C_e = \frac{-i\Delta_0 C_h(\mu - \varepsilon)H_{(\mu-\varepsilon)^2/2-1}(-q)}{H_{(\mu+\varepsilon)^2/2}(q)\varepsilon + (\mu + \varepsilon)H_{(\mu+\varepsilon)^2/2-1}(q)\sqrt{\Delta_0^2 - \varepsilon^2}}, \quad (6)$$

and the dispersion relation is given by the solutions of

$$f_{\mu+\varepsilon}(q) - f_{\mu-\varepsilon}(-q) = \frac{\varepsilon\left[f_{\mu+\varepsilon}(q)f_{\mu-\varepsilon}(-q) + 1\right]}{\sqrt{\Delta_0^2 - \varepsilon^2}} \ , \tag{7}$$

$$\text{where } f_\alpha(q) = \frac{H_{\alpha^2/2}(q)}{\alpha H_{\alpha^2/2-1}(q)} \ . \tag{8}$$

The solutions $\varepsilon_n(q)$ of Eq. (7) can be labeled with a (LL) index $n = 0, \pm 1, \pm 2, \cdots$. Figure 2 shows the zeroth LL ($n = 0$) for $\mu = 0.25\,\hbar v_F/l_B$, $0.5\,\hbar v_F/l_B$, $1.0\,\hbar v_F/l_B$, and $1.5\,\hbar v_F/l_B$ for $\Delta_0 = 5\hbar v_F/l_B$. For $\mu = 0$, we obtain the familiar dispersionless LLs at 0, $\pm\sqrt{2}\,\hbar v_F/l_B$, $\cdots$ [36]. Away from the edge the various LLs saturate at $\sqrt{2}(\hbar v_F/l_B)\mathrm{sgn}(n)\sqrt{|n|} - \mu$ for $q \to -\infty$ and $\sqrt{2}(\hbar v_F/l_B)\mathrm{sgn}(n)\sqrt{|n|} + \mu$ for $q \to \infty$. This suggests that an interesting regime can be reached by increasing μ, so that $n = \pm 1$ levels start contributing to the low-energy excitations of the system (as shown in Ref. [33]). When the chemical potential μ is finite (as measured from the charge-neutrality point of the free Dirac system), the LLs acquire a dispersion around $q = 0$ that signals the existence of Andreev edge excitations [37, 36].

For the special case of $\varepsilon = 0$ and $q = 0$, we obtain $C_h = iC_e$, and this zero-energy state can then be expressed as

$$\Psi_{00}(x) = C_e e^{-\frac{x^2}{2}} \begin{pmatrix} -i\mu H_{\mu^2/2-1}(x)e^{i\phi/2} \\ H_{\mu^2/2}(x)e^{i\phi/2} \\ iH_{\mu^2/2}(x)e^{-i\phi/2} \\ \mu H_{\mu^2/2-1}(x)e^{-i\phi/2} \end{pmatrix} . \tag{9}$$

The particle-hole-conjugation operator is given by $\Xi = \sigma_y \tau_y \mathcal{K}$ [30], where σ_j and τ_j are again the Pauli matrices acting on spin and particle-hole space respectively, and $\mathcal{K}$ symbolizes complex conjugation. Straightforward verification establishes $\Xi\Psi_{00} = -i\Psi_{00}$, and $\Xi\Xi\Psi_{00} = \Psi_{00}$. Hence the state Ψ_{00} is a Majorana fermion.

4. Chiral Majorana mode in our sample geometry

A general symmetry property [40] of the DBdG equation mandates that, for any eigenstate Ψ_{nq} with excitation energy ε_{nq}, its particle-hole conjugate $\Xi\,\Psi_{nq}$ in Nambu space is also an eigenstate and has excitation energy $-\varepsilon_{nq}$. This symmetry implies that the zero-energy state with quantum numbers $n = 0$ and $q = 0$ is its own particle-hole conjugate in our system, thus exhibiting the defining property of a Majorana fermion [1, 2]. While the Majorana state $\Psi_{00}(\mathbf{r})$ has a localized spatial profile in the direction perpendicular to the S–N junction (i.e., along the x–axis), it is completely delocalized in the direction parallel to the S–N interface. Similarly, one can show the existence of the chiral Majorana edge excitation all around the boundary of the S region, as is required by the particle-hole symmetry at zero energy. Thus the CMM encloses the entire S region that is created on the TI surface via the proximity effect. In principle, the S region may include n_v vortices, each supporting a Majorana bound state (MBS) at zero energy. The coupling between these MBSs and the CMM discussed above decays
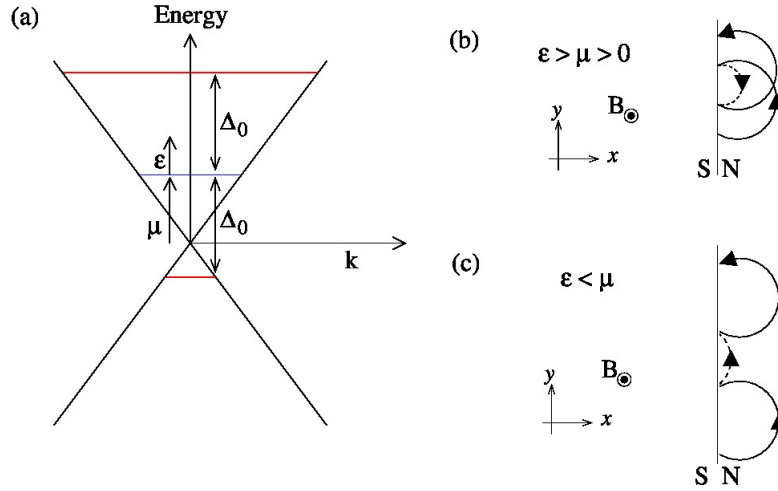
Figure 3. Semiclassical picture of Dirac-Andreev edge states [36]. (a) Conical dispersion relation representing the surface states of the TI, consisting of a top cone (conduction band) and a symmetric bottom cone (valence band), which touch at the Dirac point. A proximity-induced superconducting gap of $2\Delta_0$ opens up at the chemical potential μ. (b) If the excitation energy $\varepsilon > \mu$, the electron and the Andreev-reflected hole belong to the conduction and valence band, respectively, and the edge channel is not chiral. (Solid and dashed lines represent electron and hole trajectories, respectively.) (c) If $\varepsilon < \mu$, electrons and Andreev-reflected holes belong to the same band, and their skipping orbits form a chiral Andreev edge channel.

exponentially as a function of their spatial separation. Thus the presence of vortices will not affect the Majorana edge mode in the typical situation where the vortices are located far from the edge.

The chiral Majorana edge excitation is characterized by its velocity v_M. As the chemical potential approaches zero, the edge dispersion of the zeroth LL flattens out, implying a very small Majorana-mode velocity ($v_M \sim 0$). On the other hand, increasing the chemical potential sharpens that edge dispersion and increases v_M (see Fig. 2). In previously considered situations where CMMs emerge [31], the Majorana-mode velocity could be adjusted by changing the magnitude of the magnetization in a ferromagnetic insulator. However this is rather difficult to perform experimentally. Our setup offers a more controllable route to tune this velocity by changing the magnitude of the external magnetic field.

The semiclassical cyclotron trajectories of electrons and Andreev reflected holes for this system are shown in Fig. 3, where we consider a finite positive value of μ. Figure 3(a) shows the conical dispersion relation describing the topologically protected surface states of the TI. Due to the proximity effect a gap of magnitude $2\Delta_0$ opens up at μ. First we consider $\Delta_0 > \mu$. In this regime, there exist two kinds of cyclotron trajectories. In the first case $\epsilon > \mu$ shown in Fig. 3(b), the electron and its conjugate Andreev-reflected hole are from different (conduction and valence) bands defined with respect to the Dirac point. The semiclassical cyclotron trajectories for the electrons
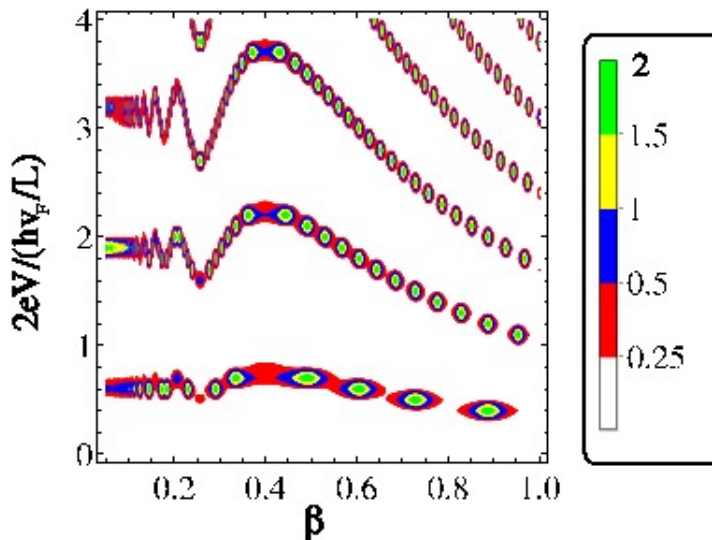
Figure 4. Contour plot of the differential conductance $(dI/dV)/(e^2/h)$ as a function of the dimensionless magnetic field denoted by $\beta = \sqrt{\hbar|eB|}v_F/\Delta_0$, and eV measured in units of $\pi\hbar v_F/L$. The reflection amplitude r_0 of the locally coupled normal lead is set to 0.9, the chemical potential is chosen to be $\mu = 0.5\Delta_0$, and the S region encloses an even number of vortices.

and the Andreev-reflected holes in this case travel in opposite direction. In the second case $\epsilon < \mu$, both the electron and its conjugate Andreev-reflected hole belong to the same (e.g., the conduction) band and move in the same direction. The chiral modes we discuss belong to the latter situation and are present even if $\Delta_0 < \mu$. However, by increasing Δ_0, we can realize a regime with multiple LLs within the gap. In this regime the coupling between the nearest LLs enriches the dynamics of the system. The low-energy excitations (close to the chemical potential) can then be described by an effective envelope-function Hamiltonian including $n = 0$ and ± 1, as discussed in Ref. [33].

5. Conductance of the CMM interferometer

The differential conductance of our setup (as shown in Fig. 1) can be calculated within the scattering matrix formalism [41, 42]. Ignoring the coupling between the MBSs and the chiral Majorana edge state enclosing the S region, the effect of vortices is to account for an additional contribution $\phi_v = n_v\pi$ to the total phase ϕ that the chiral Majorana edge fermion picks up after traversing the entire boundary of the S region. Including an additional phase of π coming from the Berry phase and the dynamic phase, the total phase acquired during a round trip is

$$\phi = n_v\pi + \pi + \frac{EL}{\hbar v_M} \,, \tag{10}$$

where L is the circumference of the S region and E is the energy of the propagating CMM state. The normal lead in this setup plays the role of both the electron and hole lead. The tunneling current from the lead to the grounded superconductor can
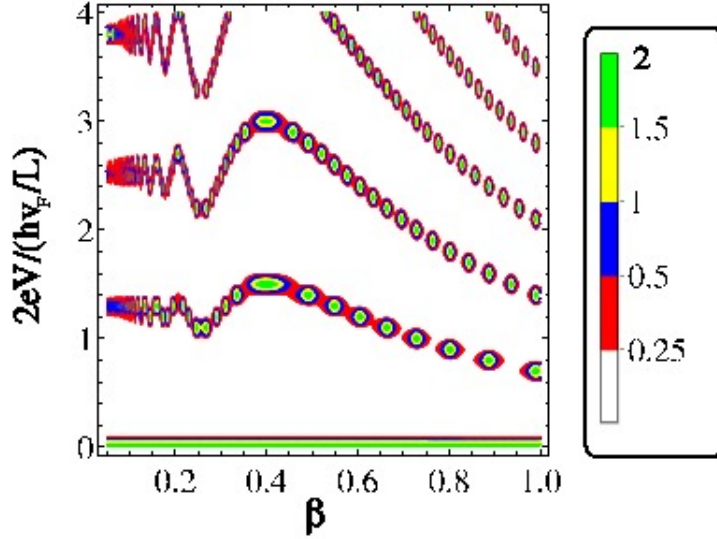
Figure 5. Same as Fig. 4, but for odd number of vortices.

be calculated straightforwardly by working in the Majorana basis [42]. An incoming electron or hole from the normal lead can be expressed in terms of *artificial* Majorana modes η_1 and η_2. In the Majorana basis, only one of the Majorana modes in the normal lead (η_1 or η_2) is coupled to the CMM going around the S region, the other is reflected with amplitude 1 [42]. Accounting for multiple reflections of the Majorana mode in the lead, the scattering matrix in the Majorana basis is [42]

$$\mathcal{S}_M = \begin{pmatrix} r_1 & 0 \\ 0 & r_2 \end{pmatrix}, \tag{11}$$

where $r_2 = 1$, and

$$r_1 = \frac{r_0 - e^{i\phi}}{1 - r_0 e^{i\phi}}, \tag{12}$$

with r_0 being the local reflection amplitude of η_1 at the junction [42]. At zero temperature, the time-averaged current from the normal lead to the grounded superconductor is [42]

$$I = \frac{e}{h} \int_0^{eV} \left(1 - Re[r_1 r_2^*]\right) dE. \tag{13}$$

We calculate the differential conductance of our setup by numerically evaluating the velocity of the CMM in the zeroth LL,

$$v_M = \hbar^{-1} \frac{d\varepsilon_n(q)}{dq}\bigg|_{q \to 0}. \tag{14}$$

We assume that v_M is constant all around the S region and determine it from the solution of Eq. (7). Figure 4 shows a contour plot of the differential conductance (dI/dV) in units of e^2/h as a function of the dimensionless magnetic field $\beta = \sqrt{\hbar|eB|}v_F/\Delta_0$, and eV measured in units of $\pi\hbar v_F/L$. The chemical potential is chosen to be
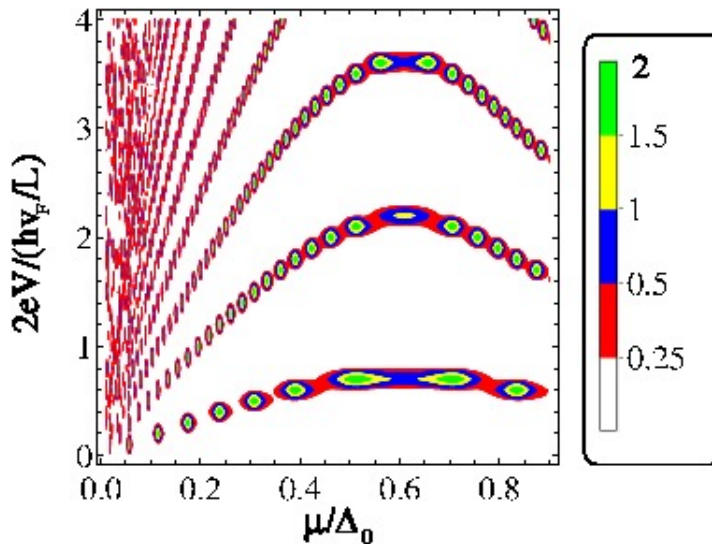
Figure 6. Contour plot of the differential conductance $(dI/dV)/(e^2/h)$ as a function of μ/Δ_0 and eV measured in units of $\pi\hbar v_F/L$. The dimensionless measure $\beta = \sqrt{\hbar|eB|}v_F/\Delta_0$ of the magnetic field is set to 0.5. Moreover, the S region encloses an even number of vortices and $r_0 = 0.9$.

$\mu = 0.5\Delta_0$, $r_0 = 0.9$, and we consider an even number of vortices. The apparent highly nonlinear behavior arises from the Majorana-fermion induced resonant Andreev reflection (MIRAR) [18] in conjunction with the variation of v_M as the magnitude of magnetic field changes. The differential conductance is periodic in eV, and the period depends on the CMM velocity. The nonlinear behavior due to MIRAR along the eV axis was investigated in detail in Ref. [18]. In our setup, dI/dV shows a nonlinear oscillating behavior as a function of the magnetic-field-dependent parameter β also. The origin of these oscillations can be traced back to the magnetic-field dependence of v_M as shown in Ref. [33]. Recent studies [34] have indicated that such a velocity modulation could be used as a pump parameter in an adiabatic-quantum-pumping setup where the pumped current is induced by the CMM.

We have also calculated the differential conductance for the case of an odd number of vortices present in the S region, see Fig. 5. In the zero-bias limit, $dI/dV|_{eV\to0} \to 2e^2/h$. In contrast, for the case of an even number of vortices shown in Fig. 4, $dI/dV|_{eV\to0} \to 0$. It has been suggested that this jump in conductance with the parity of the number of vortices is a clear signature of the Majorana mode [18].

Along similar lines we calculate the differential conductance for our setup for a fixed value of magnetic field $\beta = \sqrt{\hbar|eB|}v_F/\Delta_0 = 0.5$, as a function of μ and eV. The results are shown in Fig. 6 for an even number of vortices, and in Fig. 7 for an odd number of vortices. In the zero bias limit, we once again observe a jump in the differential conductance from $2e^2/h$ to 0 when the number of vortices changes from odd to even. We also observe oscillations as the chemical potential changes which can be traced back to oscillations in v_M [33].
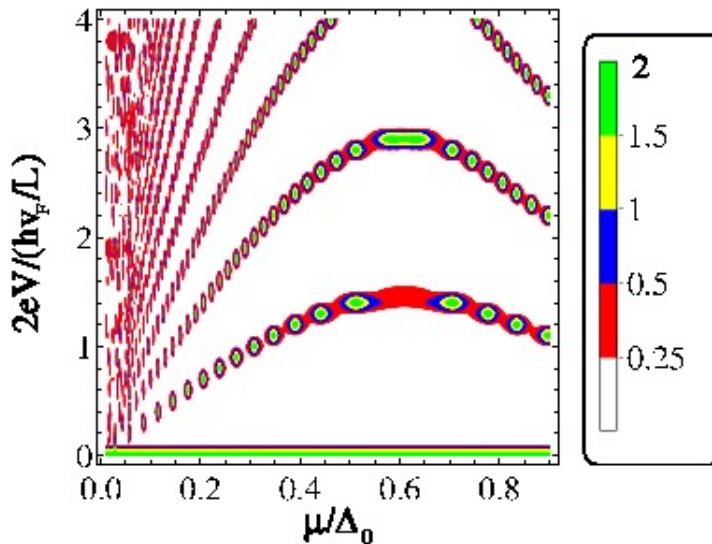
Figure 7. Same as Fig. 6, but for odd number of vortices.

6. Discussion and summary

Finally, we would like to comment upon the experimental feasibility of realizing the device setup suggested here. Using typical values such as $\Delta_0 = 0.7$ meV [43], $v_F = 5 \times 10^5$ m/s [43], and a magnetic field of 1 T, we obtain $\hbar v_F / l_B \sim 10$ meV, implying that the observation of the CMM discussed here is within the reach of current experimental efforts. However, realizing a regime with multiple LLs within the gap necessitates an increase in the proximity-induced superconducting gap Δ_0. To ensure that a finite temperature T does not completely smear out the effects we discussed, we have to ensure that $k_B T \ll \{\Delta_0, \hbar v_F / l_B, \mu\}$, where k_B is the Boltzmann constant. Therefore, measurements at sub-Kelvin temperatures will be required for these experiments.

We have ignored disorder in our calculation. Disorder in the system will result in fluctuations of the Dirac-point energy which will translate into a spatially varying chemical potential. Majorana excitations will still exist but be subject to a fluctuating velocity. Due to the topological nature of the chiral Majorana edge excitation we expect its largely unimpeded propagation even under such circumstances. In the limit of strong disorder the fluctuations in the Majorana mode velocity may suppress the oscillations described in Figs. 4 – 7.

In addition to creating the S region via the proximity effect, the planar contact with a superconducting material on top of the TI surface is likely to also induce band bending in the TI surface state beneath it. In the likely case where the resulting potential gradient is smooth on the scale of the magnetic length, the electronic structure of the Majorana mode discussed here will be largely unaffected. Furthermore, as normal reflection is suppressed for states with guiding centers close to the interface because of Klein tunneling [44], the Majorana-mode velocity will, in general, be most dominantly determined by Andreev reflection.

Our theory applies to a situation without vortices or a small number of them, i.e., for magnetic fields below or just above the first critical field B_{c1} of the superconductor. For $B < B_{c1}$, there are no vortices in the superconducting region, and the conductance for this case corresponds to that shown in Figs. 4 and 6. For fields just above B_{c1}, the vortices will be separated by distances larger than the magnetic penetration depth λ. For large $\kappa = \lambda/\xi$, where ξ is the coherence length of the superconductor, the coupling between the MBSs at the vortices can be safely ignored. However, if $\kappa \sim 1$, the hybridization between MBSs within the vortices can change our results significantly. From the basic relations between B_{c1} and the thermodynamical critical field B_c, in the large-κ-limit, and between B_c and the condensation energy [45], the above considerations impose a limiting condition on the dimensionless magnetic-field-dependent parameter β used in our calculations,

$$\beta \lesssim \frac{\ln\kappa}{\kappa} \sqrt{\frac{\mathcal{N}[(eV\,nm^3)^{-1}]}{B_{c1}[T]}} \quad . \tag{15}$$

Here $\mathcal{N}$ is the normal-state density of states at the Fermi energy for the superconducting material. In available materials systems, the right-hand side of Eq. (15) can be larger than 1. Thus our theoretical description is valid for the range of values of β shown in Figs. 4 and 5.

In conclusion, we have studied quantum transport in a superconductor–topological-insulator hybrid structure in the presence of a perpendicular magnetic field. We have shown that Landau quantization results in the emergence of a tunable chiral Majorana mode at the edge of the superconducting region induced on the surface of the topological insulator. We find that the velocity of this mode can be tuned by changing the magnitude of the external magnetic field and/or the chemical potential of the superconductor. The velocity tunability gives rise to unique signatures in the differential conductance of the system when the Majorana edge mode is coupled to a normal electronic lead. Experimental verification of the tunability of the velocity and the detailed structure of the differential conductance will provide a new platform to explore Majorana physics.

References

[1] Wilczek F 2009 *Nature Phys.* **5** 614–618
[2] Alicea J 2012 *Rep. Prog. Phys.* **75** 076501
[3] Leijnse M and Flensberg K 2012 *Semiconductor Science and Technology* **27** 124003
[4] Beenakker C 2013 *Annual Review of Condensed Matter Physics* **4** 113–136
[5] Franz M 2013 *Nature Nanotechnology* **8** 149–152
[6] Stanescu T D and Tewari S 2013 *Journal of Physics: Condensed Matter* **25** 233201

  [7] Moore G and Read N 1991 *Nucl. Phys. B* **360** 362 – 396
  [8] Stern A 2010 *Nature* **464** 187–193
  [9] Ivanov D A 2001 *Phys. Rev. Lett.* **86**(2) 268–271
 [10] Mackenzie A P and Maeno Y 2003 *Rev. Mod. Phys.* **75**(2) 657–712
 [11] Das Sarma S, Nayak C and Tewari S 2006 *Phys. Rev. B* **73**(22) 220502
 [12] Tewari S, Das Sarma S, Nayak C, Zhang C and Zoller P 2007 *Phys. Rev. Lett.* **98**(1) 010506
 [13] Sau J D, Lutchyn R M, Tewari S and Das Sarma S 2010 *Phys. Rev. Lett.* **104**(4) 040502
 [14] Sau J D, Tewari S, Lutchyn R M, Stanescu T D and Das Sarma S 2010 *Phys. Rev. B* **82**(21) 214509
 [15] Alicea J 2010 *Phys. Rev. B* **81**(12) 125318
 [16] Sengupta K, Žutić I, Kwon H J, Yakovenko V M and Das Sarma S 2001 *Phys. Rev. B* **63**(14) 144531
 [17] Bolech C J and Demler E 2007 *Phys. Rev. Lett.* **98**(23) 237002
 [18] Law K T, Lee P A and Ng T K 2009 *Phys. Rev. Lett.* **103**(23) 237001
 [19] Flensberg K 2010 *Phys. Rev. B* **82**(18) 180516
 [20] Mourik V, Zuo K, Frolov S M, Plissard S R, Bakkers E P A M and Kouwenhoven L P 2012 *Science* **336** 1003–1007
 [21] Das A, Ronen Y, Most Y, Oreg Y, Heiblum M and Shtrikman H 2012 *Nature Physics* **8** 887–895
 [22] Deng M T, Yu C L, Huang G Y, Larsson M, Caroff P and Xu H Q 2012 *Nano Letters* **12** 6414–6419
 [23] Finck A D K, Van Harlingen D J, Mohseni P K, Jung K and Li X 2013 *Phys. Rev. Lett.* **110**(12) 126406
 [24] Lee E J H, Jiang X, Houzet M, Aguado R, Lieber C M, De Franceschi S 2014 *Nature Nanotechnology* **9** 79–84
 [25] Kitaev A Y 2001 *Physics-Uspekhi* **44** 131
 [26] Rokhinson L P, Liu X and Furdyna J K 2012 *Nature Physics* **8** 795–799
 [27] Williams J R, Bestwick A J, Gallagher P, Hong S S, Cui Y, Bleich A S, Analytis J G, Fisher I R and Goldhaber-Gordon D 2012 *Phys. Rev. Lett.* **109**(5) 056803
 [28] Hasan M Z and Kane C L 2010 *Rev. Mod. Phys.* **82**(4) 3045–3067
 [29] Qi X L and Zhang S C 2011 *Rev. Mod. Phys.* **83**(4) 1057–1110
 [30] Fu L and Kane C L 2008 *Phys. Rev. Lett.* **100**(9) 096407
 [31] Fu L and Kane C L 2009 *Phys. Rev. Lett.* **102**(21) 216403
 [32] Tanaka Y, Yokoyama T and Nagaosa N 2009 *Phys. Rev. Lett.* **103**(10) 107002
 [33] Tiwari R P, Zülicke U and Bruder C 2013 *Phys. Rev. Lett.* **110**(18) 186805
 [34] Alos-Palop M, Tiwari R P and Blaauboer M 2013 *ArXiv e-prints* (*Preprint* 1305.1512)
 [35] Park S, Moore J E and Sim H S 2013 *ArXiv e-prints* (*Preprint* 1307.7484)
 [36] Akhmerov A R and Beenakker C W J 2007 *Phys. Rev. Lett.* **98**(15) 157003
 [37] Hoppe H, Zülicke U and Schön G 2000 *Phys. Rev. Lett.* **84**(8) 1804–1807
 [38] Zülicke U, Hoppe H and Schön G 2001 *Physica B* **298** 453–456
 [39] Giazotto F, Governale M, Zülicke U and Beltram F 2005 *Phys. Rev. B* **72** 054518
 [40] de Gennes P G 1989 *Superconductivity of Metals and Alloys* (Reading, MA: Addison-Wesley)
 [41] Nazarov Y and Blanter Y 2009 *Quantum Transport: Introduction to Nanoscience* (Cambridge University Press)
 [42] Li J, Fleury G and Büttiker M 2012 *Phys. Rev. B* **85**(12) 125440
 [43] Zhang D, Wang J, DaSilva A M, Lee J S, Gutierrez H R, Chan M H W, Jain J and Samarth N 2011 *Phys. Rev. B* **84**(16) 165120
 [44] Culcer D 2012 *Physica E* **44** 860–884
 [45] Tinkham M 1996 *Introduction to Superconductivity* Second Ed. (McGraw-Hill)